Active, long-lived upper-plate splay faulting revealed by thermochronology in the Alaska subduction zone

Suoya Fan, Kristin Morell, Donald Fisher, Hugues Raimbourg, Vincent Famin, Kristijan Rajič

Active, long-lived upper-plate splay faulting revealed by thermochronology in the Alaska subduction zone

Suoya Fan[1], Kristin D. Morell[1], Donald M. Fisher[2], Hugues Raimbourg[3], Vincent Famin[4,5], Kristijan Rajič[6]

1. Department of Earth Science, University of California, Santa Barbara, Santa Barbara, CA, USA
2. Department of Geosciences, Pennsylvania State University, University Park, PA, USA.
3. Institut des Sciences de la Terre d'Orléans, Université d'Orléans/CNRS/BRGM UMR7327, 1A Rue de la Ferollerie, Orléans 45100, France
4. Université Paris Cité, Institut de Physique du Globe de Paris, Paris, France
5. Laboratoire Géosciences Réunion, Université de La Réunion, Saint-Denis, France
6. Department of Earth Sciences, Durham University, Science Laboratories, South Road, Durham DH1 3LE, UK

Keywords:

Splay Fault; Forearc Tectonics; Alaska Subduction Zone; Thermochronology; Exhumation History

Highlights:

- Exhumation history revealed by thermochronology in the Alaska forearc region
- Inboard persistent deformation along a highly active forearc splay fault since 6-7 Ma
- Long-term slip rate and deep geometry estimations of the Kodiak Shelf Fault
- Upper-plate architecture may control splay fault development and long-term activity

Abstract

The lack of subaerial forearc geological records in active subduction zones has hindered our understanding of the roles of upper-plate structures and their interactions with plate interface processes in accommodating forearc deformation. Forearc splay faults, a type of upper-plate structure, are of particular interest due to their high efficiency in triggering tsunamis during great earthquakes. The coastal area of the Kodiak Islands exhibits stratigraphic and geomorphologic records of Miocene to Recent vertical tectonism and Quaternary thrust faults, suggesting potential splay-fault-involved deformation over geological timescales. To better understand the mechanisms of forearc long-term strain accumulation and the roles of splay faults, we investigate the spatial and temporal pattern of recent forearc exhumation in the Kodiak accretionary prism by conducting zircon and apatite (U-Th)/He (ZHe and AHe) thermochronologic analyses and thermal history modeling. These results are supplemented by field investigations, detrital zircon geochronology analyses and offshore active fault mapping. Most of our ZHe ages record cooling through ZHe closure temperature in the late Eocene-early Oligocene, temporally and spatially consistent with the Eocene-early Oligocene broad antiformal exhumation previously documented by zircon and apatite fission track thermochronological ages. However, our AHe ages record cooling through AHe closure temperature from early Miocene to Pliocene and exhibit an overall trenchward younging trend, with all the Pliocene ages (3-5 Ma) from the trench edge of the island. Our thermal history modeling and field survey suggest that the trenchward coastal area of the Kodiak Islands experienced a change from the early-middle Miocene basin subsidence to recent deformation and rapid uplift since 6-7 Ma to recent, while the rest of the islands experienced an early-middle Miocene decrease in the prolonged exhumation from the Eocene-Oligocene. The newly revealed long-term exhumation pattern resembles the estimated uplift

patterns based on elevated marine terraces and geodetic data. The early-middle Miocene change in the exhumation pattern might be caused by a change in the dominant deformation mechanism affecting the Kodiak Islands, from broad underplating along the subduction interface mainly during the Eocene-Oligocene to hanging-wall uplift due to an active crustal splay thrust fault system since the late Miocene (the Kodiak Shelf Fault). We further discuss the dip-slip rate and geometry of the Kodiak Shelf Fault system and how inherited forearc upper-plate structures and lithology may affect forearc fluid distribution and facilitate the development and persistent deformation of the Kodiak Shelf Fault system.

1. Introduction

Investigating the long-term activity, geometry, lifespan, and evolution of forearc upper-plate structures in subduction zones is critical to understanding the growth mechanisms of accretionary complexes, which involve complex and dynamic interactions between plate-interface and upper-plate processes. Many studies have aimed to better understand these interactions by correlating upper-plate structures, topography, and basins with subduction interface properties and earthquake patterns (e.g., Wells et al., 2003; Saillard et al., 2017; Dielforder et al., 2020; Jolivet et al., 2020; Michel-Wolf et al., 2022; Oryan et al., 2024). Deep-rooted crustal splay faulting, for example, is a major thickening mechanism in the forearc, as indicated by out-of-sequence thrusts archived in exposed forearc accretionary complexes, such as the Kodiak accretionary complex (Rowe et al., 2009; Farris, 2010; Wilson, 2013). The active equivalents of these faults, forearc active splay faults, tend to be located near the rheological transition at the up-dip edge of the seismogenic zones (Wang and Hu, 2006; Kimura et al., 2007; Wang and Morgan, 2022). This observation, along with records of their direct involvement in tsunami-triggering processes during great earthquakes, further highlights the significance of

70 understanding active splay faults in assessing seismic-tsunami hazards (e.g., Plafker, 1965;
71 Cummins and Kaneda, 2000; Sibuet et al., 2007). However, the long-term history, including,
72 initiation, lifespan, cessation, and reactivation of currently active splay faults, is rarely well
73 studied.

74 Splay faults have been proposed to efficiently transfer deep displacement to the surface,
75 fostering tsunami genesis (Moore et al., 2007; Wendt et al., 2009; van Zelst et al., 2022).
76 Previous studies suggest that the coseismic rupture of a forearc splay fault in the Prince William
77 Sound fostered the genesis of a large tsunami in the Alaska subduction zone during the 1964
78 M9.2 Great Alaska earthquake (Plafker, 1965; Suito and Freymueller, 2009; Suleimani and
79 Freymueller, 2020) and its repeated ruptures have contributed to long-term permanent forearc
80 uplift (Liberty et al., 2013; Haeussler et al., 2015; DePaolis et al., 2024). The involvement of
81 splay fault rupture has also been suggested in other great tsunamigenic subduction zone
82 earthquakes, such as the 1944 M8.1 Tonankai earthquake and the 1946 M8.3 Nankai earthquake
83 in Japan (Cummins and Kaneda, 2000; Park et al., 2002) as well as the 2004 Mw9.2 Sumatra
84 earthquake (Sibuet et al., 2007).

85 Splay faults located in the general region near the up-dip edge of the seismogenic zone
86 have been well-documented, with examples such as Nankai (Park et al., 2002; Kimura et al.,
87 2007; Moore et al., 2007; Strasser et al., 2009), Sumatra (Cook et al., 2014; Qin et al., 2024), and
88 Hikurangi (Barker et al., 2018; Barnes et al., 2020). Similarly, offshore surveys in the Alaska
89 subduction zone have primarily focused on the forearc frontal part straddling the up-dip limit of
90 the seismogenic zone (e.g., Li et al., 2018; von Huene et al., 2021). However, the geometry and
91 long-term evolution of active splay faults located in the forearc farther inboard are generally

92 poorly understood, in large part because direct geological studies of these structures are often
93 hindered by a lack of subaerial exposures and require deep seismic data.
94 The Kodiak Islands in the forearc of the highly-coupled Alaska subduction zone, about
95 140 km from the trench, is an ideal area to probe the geometry and rates of splay faulting in the
96 inner forearc. The trenchward coastal area of the Kodiak Islands is located approximately above
97 the present down-dip edge of the seismogenic zone and exhibits stratigraphic and
98 geomorphologic records of Miocene to Recent vertical tectonism and includes a series of
99 Quaternary active faults (e.g., Clendenen et al., 1992; Carver et al., 2008; Elliott and
100 Freymueller, 2020). These active faults are interpreted as a part of the Kodiak Shelf Fault Zone,
101 a major offshore crustal splay fault zone that has been proposed to have ruptured during the 1964
102 Great Alaska earthquake and was the potential source of a local Kodiak Islands tsunami (Ramos
103 et al., 2022). These co-located indicators of forearc deformation across a wide range of
104 timescales suggest a potential causal relationship between the persistent activity of the Kodiak
105 Shelf Fault Zone and long-term upper-plate vertical tectonism, as evidenced by uplifted and
106 deformed Miocene shelf-basin strata. However, testing this hypothesis requires a better
107 understanding of the Kodiak Shelf Fault Zone, including its kinematics, deep geometry,
108 deformation rates, and slip history.
109 To better understand the rates, history, and spatial distribution of forearc deformation
110 across the Kodiak Shelf Fault Zone, its relation to deep accretionary complex structures and its
111 connectivity with the subduction interface, we investigate the spatial-temporal exhumation
112 patterns of the Kodiak Islands with a focus on the post-Oligocene history of the trenchward
113 coastal area. We conduct new low-temperature zircon and apatite (U-Th)/He (ZHe and AHe)
114 thermochronology analyses together with thermal history modeling and detrital zircon

geochronologic analyses. The AHe ages reveal a previously unrecognized rapid exhumation pattern that we interpret to be primarily controlled by displacement along the Kodiak Shelf Fault Zone. The ZHe and AHe ages suggest a significant change in forearc dominant deformation style in the early-middle Miocene. The new deformation pattern after the style change indicates persistent deformation of the Kodiak Shelf Fault Zone from 6-7 Ma to present. We further infer a deep fault geometry and compare it with published forearc geophysical data to discuss how the inherited upper-plate structures and lithologic architecture may affect regional fluid distribution and facilitate the development and persistent deformation of the Kodiak Shelf Fault.

2. Geology

2.1. Tectonostratigraphy of the Kodiak Islands

The Kodiak Islands represent the subaerial part of the Kodiak accretionary complex, comprising a series of trench-parallel-striking rock packages that decrease in age and metamorphic grade trenchward (Moore et al., 1983) (Fig. 1). These rock packages were accreted episodically since the Jurassic through underplating or frontal accretion (Moore and Allwardt, 1980; Byrne and Fisher, 1987; Fisher and Byrne, 1987; Fisher and Byrne, 1992; Clendenen et al., 2003; Rajič et al., 2023). The northwestern edge of the Kodiak Islands comprises an island arc assemblage of late Triassic to early Jurassic ages and the Jurassic Raspberry Schist (Carden et al., 1977; Burns, 1985; Roeske et al., 1989). The Border Ranges Fault juxtaposes these rocks against the Uyak Complex, a tectonic mélange with rocks that contain fossils of age ranging from mid-Permian to mid-early Cretaceous (Connelly, 1978). The Uyak Complex is in tectonic contact with the Kodiak Formation southeast of it along the Uganik Thrust (Moore, 1978; Rowe et al., 2009).

The Kodiak Formation is a mostly structurally coherent, thick sequence of deep-water turbidites, including interbedded slates, siltstones, and sandstones, deposited in the Maastrichtian ~70 Ma ago (Byrne and Fisher, 1987; Sample and Reid, 2003). It occupies most of the Kodiak Islands and forms a regional anticlinorium (Sample and Moore, 1987; Fisher and Byrne, 1992; Rajič et al., 2023). The Kodiak Formation is separated from the Paleocene Ghost Rocks Formation by the Contact Fault (Fig. 1; Farris, 2010; Wilson, 2013). The Ghost Rocks Formation consists of a structurally coherent unit in the northwest and a tectonic mélange in the southeast (Byrne, 1984). The accretion of the Kodiak Formation and Ghost Rocks Formation occurred from the late Cretaceous to the early Paleogene (Byrne, 1984; Byrne and Fisher, 1987), and the youngest temporal limit is well bracketed by the ages of temporally close (about 58-62 Ma) but widely distributed intrusive rocks (Moore et al., 1983; Byrne and Fisher, 1987; Sample and Moore, 1987; Farris et al., 2006; Farris, 2010). These intrusive rocks are mostly andesite and granodiorite with some mafic rocks and are interpreted to be caused by the west-to-east migrating ridge subduction and the interaction of the MORB-type magmas with the metasedimentary rocks in the accretionary prism (Moore et al., 1983; Haeussler et al., 2003; Farris et al., 2006). The largest pluton is the Kodiak Batholith, the exposure of which trends sub-parallel with the long axis of the islands (Fig. 1).

The Eocene Sitkalidak Formation, in fault contact with the Ghost Rocks Formation, is a deep-sea fan sequence consisting of sandstone, siltstone, mudstone, and conglomerate and outcrops along the southeastern edge of the Kodiak Islands (Figs. 1 and 2), including the Ugak Island in our study area (Nilsen and Moore, 1979; Moore and Allwardt, 1980). It contains two structural units: a less deformed portion interpreted as a shortened slope basin or slope apron deposit and a strongly deformed portion featured by landward verging folds and thrusts

160 interpreted as trench-filling sediment offscraped from the lower plate (Moore and Allwardt,
161 1980).
162 Oligocene-Pleistocene slope basin fill overlies the Ghost Rocks and Sitkalidak
163 Formations above an angular unconformity, and it contains several units of different ages along
164 the southeastern margin of the Kodiak Islands (Moore and Allwardt, 1980; Clendenen et al.,
165 1992; Marincovich and Moriya, 1992). In the Narrow Cape area, the sequence above the
166 unconformity is the slightly younger middle Miocene Narrow Cape Formation comprising
167 shallow marine sandstone and sandy siltstone, with interbedded conglomerate beds (Moore et al.,
168 1983). The age of the Narrow Cape Formation is interpreted to be 16-15 Ma based on well-dated
169 faunas (Marincovich and Moriya, 1992). The Oligocene-Miocene unconformity has been
170 interpreted to be correlated seaward to an unconformity visible in seismic reflection profiles in
171 the offshore region (Fisher and Holmes, 1980; Moore and Allwardt, 1980; Clendenen et al.,
172 1992). The offshore part of the post-unconformity basin has continuously received sediments up
173 until the present day. The current trenchward boundary of the shelf-basin is approximately
174 located at the present-day shelf break, about 60-80 km trenchward from the landward boundary
175 exposed on the Kodiak Islands. The subaerial basin recorded by the Narrow Cape Formation in
176 the Kodiak coastal area may represent the deformed and uplifted part of this same basin.
177 **2.2. Cretaceous-Cenozoic Deformation, Exhumation and Active Tectonics**
178 **2.2.1 Cretaceous to Miocene**
179 Two main episodes of deformation and exhumation before the Miocene have been
180 recognized in the Kodiak Islands. The first episode is represented by the accretion of the Kodiak
181 and Ghost Rocks Formations, mainly through underplating along the subduction interface from
182 the late Cretaceous to the early Paleocene. Evidence for underplating includes the regional

anticlinorium, duplex structures in both mesoscopic and map scales, and across-strike changes in deformation style, magnitude and structural orientation (Sample and Fisher, 1986; Fisher and Byrne, 1987; Sample and Moore, 1987; Fisher and Byrne, 1992; Rajič et al., 2023). The peak temperature and amount of exhumation experienced by the Kodiak and Ghost Rocks Formations also mimic the antiformal pattern with the highest magnitude in the core of the anticlinorium (Clendenen et al., 2003; Rajič et al., 2023). The second episode of exhumation and thickening occurred from Eocene to Oligocene and has been interpreted as a result of trenchward-propagating underplating. Evidence for this process is based on a thermochronologic study involving zircon and apatite fission track (ZFT and AFT) dating that shows cooling ages become younger trenchward from the northwestern limit of the Kodiak Formation to the Kodiak Batholith (Clendenen et al., 2003). Moreover, an offshore seismic reflection profile northeast of the Kodiak Islands exhibits arched reflectors that coincide with a thick low-velocity zone below the Mesozoic and Paleocene accretionary prism, consistent with underplating (Byrne, 1986; Moore et al., 1991; Ye et al., 1997).

2.2.2 Miocene to Quaternary

Paleoseismic, geodetic, stratigraphic, and field data together provide several lines of evidence for Quaternary-active deformation within the Narrow Cape and surrounding area of the Kodiak Islands. Geomorphology and paleoseismology surveys in the Narrow Cape area have identified several near-vertical faults that have been reported to accommodate both vertical and strike-slip Quaternary displacement (Carver et al., 2008). Carver et al. (2008) documented fault activity spanning the latest Pleistocene and Holocene and suggested the faults offset a marine terrace by up to 20 m and offset channels left-laterally by up to 30-35 m. Carver et al. (2008) interpreted the major faults as part of the Kodiak Shelf Fault Zone, a ~200-km-long margin-

parallel active splay fault system (Fig. 1). In the field, we observed these faults cross-cutting the sub-horizontal angular unconformity separating the Ghost Rocks and Narrow Cape Formations by as much as ~30 m in the sea cliff (Fig. 2). The angular unconformity and the Narrow Cape Formation above it have been gently folded into an anticline and syncline, and are likely related to these active structures. Carver et al. (2008) recognized a group of coastal surfaces, characterized by a locally uniform elevation, planar sub-horizontal abrasion surfaces, with a sharp back-edge that parallels the shoreline. They interpreted them as raised wave-cut marine terraces formed during oxygen-isotope stage 5e (130-120 ka). The elevation of these marine terraces across the Kodiak Islands also increases abruptly in the Narrow Cape area, suggesting a 3-5 times higher Quaternary uplift rate of the Narrow Cape area than areas arcward (Carver et al., 2008), although the source of this reported uplift is not described in previous literature. Campaign GNSS data collected over an 8-year period also exhibit the highest across-strike velocity spatial gradient in this region, suggesting left-lateral transpressional strain, in the Narrow Cape area (Sauber et al., 2006; Carver et al., 2008). The area also lies roughly above the locked-creeping transition zone along the subduction interface (Elliott and Freymueller, 2020).

In the trenchward offshore within 15 km of the Narrow Cape area of the Kodiak Islands, the Kodiak Shelf Fault Zone has been recognized and mapped based on seismic reflection images and bathymetry data (Ramos et al., 2022). The fault system contains multiple strands offshore, among which the most recognizable is the Ugak Thrust, located ~5 km seaward of Ugak Island (Figs. 1 and 3). Based on seismic reflection profiles, these faults have been reported to be landward dipping at 65-80° close to the seafloor and may merge at depth (Ramos et al., 2022). The Ugak Fault offsets the seafloor, forming a prominent bathymetric scarp, as much as 30 m high, and extends at least 80 km in length. Other high-angle faults have been previously

identified cutting the slope basin strata but their recent activity remains unclear (Fisher and Holmes, 1980). Northeast of the Kodiak Islands, in the Prince William Sound segment, a similar megathrust splay fault system in the equivalent structural location in the forearc has been recognized and thought to have ruptured during the 1964 M9.2 earthquake, but there is no direct evidence suggesting it connects to the Kodiak Shelf Fault Zone (Liberty et al., 2013; Haeussler et al., 2015; Liberty et al., 2019; DePaolis et al., 2024). Although these previous studies provide evidence for Quaternary activity, mainly in the form of faulting and folding in the Narrow Cape region, how long these structures have been active, their exhumation histories, throw rates, and potential relationship to the underplating and duplexing structures remain poorly understood.

3. Thermochronology and Geochronology

3.1. Methods and samples

To investigate post-Oligocene to Quaternary exhumation mechanisms of the Kodiak Islands, we conducted ZHe and AHe thermochronologic analyses on samples collected along a trench-perpendicular transect (Fig. 1; Tables 1). The closure temperatures of the zircon and apatite thermochronometers are affected by various factors, such as the chemical composition of the minerals, concentration of radiation damage, grain size and cooling rate (Reiners et al., 2004; Reiners, 2005) but typically range from ~ 170-190 °C (Reiners et al., 2004) and ~ 45-70 °C (Flowers et al., 2009). We obtained 19 ZHe and 13 AHe ages from 19 samples across the Kodiak Islands (Fig. 1 and 2; Tables 1 and S1), from the Uyak Complex along the landward coast to Ugak Island in the trenchward coastal area. We increased sampling density in the southeastern half of the transect. Our sampling strategy was to first attempt to sample 60-Ma plutonic rocks, because we found that these samples contained the largest suitable apatite and zircon grains for dating. When these rock types were not available along the transect, we also sampled low-grade

252 metamorphic rocks of the Kodiak and Ghost Rocks Formation, sandstones from the Sitkalidak
253 and Narrow Cape Formations, and two samples from the Uyak Complex. We collected samples
254 with the largest visible grain size. The supplementary information contains the details of our
255 sample processing and dating analysis.
256 In addition to thermochronology, we also conducted detrital zircon (U-Pb)
257 geochronologic analyses on two Narrow Cape samples and one Sitkalidak Formation sample to
258 understand their provenance and depositional ages. The Sitkalidak Formation sample was
259 collected from Ugak Island, and the Narrow Cape Formation samples are collected directly
260 above its unconformable contact with the Ghost Rocks Formation (Fig. 2).
261 **3.2. Results**
262 The AHe ages range from 20 Ma to 3 Ma, showing an overall decrease in age trenchward
263 for the 30-km-long area northeast of Ugak Island (Figs. 2 and 4). The ages from the Uyak
264 Complex to the Contact Fault are generally spatially invariant at 15-20 Ma for 70 km across
265 strike. Neither the Uganik thrust nor the Contact Fault show variations in cooling ages across
266 them, suggesting no significant faulting-related exhumation along these onshore major faults
267 since the Miocene. The AHe cooling ages from the plutonic rock that intruded into the Ghost
268 Rocks Formation and further trenchward are all younger than 10 Ma, and the four samples
269 closest to the offshore Kodiak Shelf Fault Zone, within 20 km from the Ugak Fault, yielded
270 Pliocene cooling ages (3-5 Ma). Two of the Pliocene cooling ages are derived from the youngest
271 grain age in each sample from the Narrow Cape Formation. These samples exhibit a wide
272 dispersion of AHe grain ages, including ages younger than the middle Miocene depositional age,
273 indicating partial thermal resetting of the samples during burial heating. Because their youngest
274 grain ages (4.1 ± 0.2 Ma and 5.1 ± 0.2 Ma) are close to the mean aliquot ages of the fully

thermally-reset Sitkalidak Formation (3.3 ± 0.3 Ma) and Ghost Rocks Formation (4.3 ± 0.6 Ma), we interpret these youngest grains as being fully or nearly fully reset before recent cooling through the AHe partial retention temperature zone.

The ZHe age range overall overlaps with the published AFT ages and are younger than the ZFT ages in the area of data coverage (>38 km on the age-distance profile in Fig. 4). These ZHe ages exhibit an overall decrease in cooling ages from 52-54 Ma for samples of the early Cretaceous Uyak Complex on the landward side of the Kodiak Islands to 30-34 Ma of the Kodiak Batholith (ca. 58-59 Ma U-Pb zircon ages; Farris, 2010). This age spatial variation pattern resembles the AFT age spatial pattern reported by Clendenen et al. (2003).

The ZHe, AFT and ZFT samples all progressively decrease in age from the arcward coast to the Kodiak Batholith. In contrast, the ZHe ages further trenchward, located about 0-38 km on the age profile (Fig. 4), are invariant in age along strike, with samples in this region close to or slightly older than the ZHe ages of the Kodiak Batholith. Among them, the five samples closest to the Ugak Thrust are not thermally reset after deposition: four samples from the Narrow Cape Formation and Sitkalidak Formation yield dispersed grain ages older than their depositional ages. One sample from the Ghost Rocks formation in the Narrow Cape area close to the unconformity generated grain ages of 60-67 Ma, much older than the ZHe ages of two other Ghost Rocks Formation samples (30 and 35 Ma) near a basalt intrusion and the ages of the pluton rock intruded into the Ghost Rocks Formation.

The U-Pb detrital zircon ages of the Sitkalidak Formation and the Narrow Cape Formation samples mostly range from 50 Ma to 220 Ma (Table S2). The probability density curve peaks at around 60 Ma, a broad high age spectrum ranging from 60 to 110 Ma, and a low broad age spectrum of 130-220 Ma, mainly straddling the Jurassic (Fig. 5). The youngest ages

298 are much older than the depositional ages of the two formations (Eocene-early Oligocene and
299 mid-late Miocene, respectively); therefore, they do not provide meaningful estimation of
300 maximum depositional ages. The 60 Ma peak coincides with the narrow age range of the widely
301 distributed igneous rocks, represented by the Kodiak Batholith. The broad high spectrum of the
302 Cretaceous ages and the low broad spectrum of the Jurassic ages can be correlated with the
303 widely distributed Cretaceous Kodiak Formation and the Jurassic accretionary complex and
304 plutons on the northwestern edge of the Kodiak Islands. Therefore, the data support the idea that
305 the Sitkalidak and Narrow Cape Formations might be mainly sourced from the Kodiak Islands
306 and record the broad exhumation of the island during their deposition from the Eocene to
307 Miocene.

308 **4. Thermal History Modeling**

309 The variations in thermochronology ages along the transect and the source-to-sink history
310 associated with the deposition of the Sitkalidak and Narrow Cape Formations, all indicate spatial
311 variations in erosion and deposition of the Kodiak Islands. To further investigate the magnitude
312 and timing of exhumation across the transect, we conducted one-dimensional thermal history
313 modeling using the HeFTy (Ketcham, 2005) program with our new data. The temperature-time
314 constraints used in the HeFTy modeling were based on geological context, published nearby
315 thermochronologic data from Clendenen et al. (2003) and peak temperature estimations from
316 Rajič et al. (2023) (Figs. 2 and 6). Considering the higher data density and higher cooling age
317 contrast in the southeastern half of the Kodiak Islands, we selected five modeling localities
318 between the Kodiak Batholith, where the minimum ZHe, AFT, and ZFT ages have been
319 reported, and the Ghost Rocks Formation in the trenchward coastal area of the islands, where the
320 youngest AHe ages are located (Fig. 4). Models 1 and 2 are the farthest and of similar distance

from the trench, but they are 43 km apart along strike. Models 2 to 5 are progressively closer to the trench. For detailed descriptions, modeled age data, thermal history constraints, and the geological context considered in each model, refer to the text and Table S3 in the Supplementary Information.

The thermochronologic data and modeling results show that the previously recognized Eocene-Oligocene broad cooling lasted until the early Miocene (20-15 Ma). After that, the trenchward coastal area and the central part of the Kodiak Islands exhibit distinct thermal histories. During approximately the middle-late Miocene, the central part of the Kodiak Islands (Models 1-3) changed to a slow cooling path, while the trenchward coastal area (Models 4 and 5), mainly the area of Ghost Rocks Formation and Narrow Cape Formation, experienced a transition from cooling to reheating, which was associated with the change from erosion to deposition along the angular unconformity beneath the forearc basin sediments of the Narrow Cape Formation. Some good-fit temperature-time paths suggest a possible short period of accelerated cooling during the transitional phase (around 20-15 Ma) preceding the slow cooling phase in the central part of Kodiak Islands; but this possible acceleration in cooling is not required in all good-fit temperature-time paths. Since the latest Miocene, the trenchward coastal area of the islands has been experiencing rapid cooling.

5. Discussion

5.1. Exhumation History

Our new ZHe ages and published ZFT and AFT ages are consistent with the previous interpretation that the Kodiak Islands experienced broad antiformal thickening and exhumation from the Eocene to Oligocene that straddles the Kodiak Islands (Clendenen et al., 2003). Structural and geophysical observations suggest the underplating process might have caused this

regional thickening and exhumation pattern with a hinge line located in the central part of the Kodiak Islands (e.g., Byrne, 1986; Fisher and Byrne, 1992; Ye et al., 1997). Our ZHe ages and fission track ages of previous researchers (Clendenen et al., 2003) agree with this pattern as evidenced by their across-strike long-wavelength gradual change with the youngest ages in the Kodiak Batholith area in the central part of the Kodiak Islands (Fig. 4). This interpretation is further supported by Raman spectroscopy of carbonaceous materials that reveals a similar pattern of peak temperature: relatively high temperature records broadly distributed in the central part of the Kodiak Islands with decreased temperature records in both trenchward and landward coastal areas (Rajič et al., 2023).

Our new AHe ages reveal a previously unrecognized cooling age pattern along the transect (Fig. 4). In the northwest, the AHe ages are relatively invariant, ranging from 15-20 Ma for ~60 km across strike from the Uyak Complex to the Kodiak Batholith. Moving trenchward, in the area occupied by the Ghost Rocks mélange and Narrow Cape Formations, the ages decrease to 4-5 Ma. Finally, at Ugak Island, about 5 km from the Ugak Fault, the AHe ages further decrease to 3 Ma. This AHe age pattern suggests that the previously recognized Eocene-Oligocene broad exhumation might have extended into the early Miocene in the central part of the Kodiak Islands, but the late Miocene-Pliocene exhumation may have been affected by a different deformation mechanism than the Eocene to Oligocene underplating.

The difference in uplift and subsidence history between the trenchward coastal area of the Kodiak Islands and the area to the arcward is investigated with our one-dimensional thermal history models that incorporate constraints from geological observations (Fig. 6). In the area landward of the Contact Fault, represented by Models 1-3, the prolonged cooling in the Paleogene lasts through the Miocene. However, the cooling rate decreased after the early-middle

Miocene (20-15 Ma) and has since maintained a slow cooling rate. In the meantime, the trenchward coastal area of the Kodiak Islands, the area represented by Models 4 and 5, experienced a more complicated thermal history involving two cooling phases interrupted by a reheating process.

The first cooling episode of the trenchward coastal area of the Kodiak Islands might be caused by exhumation associated with the prolonged Oligocene to Miocene broad antiformal folding event, which may be related to underplating (Fig. 4). The unconformity between the Ghost Rocks and the Narrow Cape Formations, indicating uplift and erosion prior to the middle Miocene, may have formed during this period. The reheating process in Models 4 and 5 corresponds to the deposition of the Narrow Cape Formation, a subsidence and burial event, and temporally overlaps with the transition from fast to slow cooling in Models 1-3 (Fig. 6). These models suggest that the shelf subsidence in the Narrow Cape area indicated by the Narrow Cape basin formation is synchronous with a decrease, if not cessation, of the underplating process northwest of the basin below the Kodiak Islands. Previous stratigraphic and lithologic data of the shelf basin (Clendenen et al., 1992), our new detrital zircon U-Pb age spectrum, and the overlap between the range of the detrital ZHe ages of the Narrow Cape Formation and the cooling age range landward of the shelf basin, all suggest that the Kodiak Islands is the main source of sediment in the shelf basin along the Kodiak Islands coast in this period.

The second rapid cooling episode after the mid-late Miocene deposition and reheating along the trenchward coast of the Kodiak Islands (Models 4 and 5) is missing in the area represented by Models 1-3 (Fig. 6). Our thermal modeling results suggest that the initiation of this exhumation episode is no later than ~6 Ma (Fig. 6). The youngest basin fill along the Kodiak Islands coast, the late Pliocene-Pleistocene Tugidak Formation, locally overlies the along-strike

equivalent of the Narrow Cape Formation on the Trinity Island about 150 km southwest of our study area (Clendenen et al., 1992), suggesting that the initiation time of the latest rapid coast uplift should not be much older than the late Pliocene. The latest Miocene Albatross sedimentary sequence, the shelf basin record on the Trinity Islands, records a transition from a shallow-marine depositional environment to a terrestrial environment suggesting an uplift process (Clendenen et al., 1992). These observations bracket the initiation time of the rapid uplift and exhumation at about 6-7 Ma.

5.2. Miocene-Quaternary Exhumation Pattern and the Kodiak Shelf Fault Zone

Assuming a thermal gradient of about 30 °C/km (Moore and Allwardt, 1980) and a peak temperature of 120 °C (Rajič et al., 2023) results in an exhumation rate of ~0.6-0.7 mm/yr and total exhumation of about 4 km for the Miocene-Quaternary episode. This estimated exhumation rate is close to the inferred uplift rate of about 0.75 mm/yr based on the elevation of the uplifted coastal surface, assuming the surface formed during 130–120 ka (Carver et al., 2008).

To better evaluate the spatial variation in the new Miocene-Recent exhumation pattern revealed by the AHe ages, we calculated the exhumation rate for each AHe sample assuming steady, vertical rock uplift and unchanging topography (van der Beek and Schildgen, 2023). The results represent the averaged exhumation rate since the samples cooled through their closure temperatures. In three calculations, we assumed three initial geothermal gradients at 25 °C/km, 30 °C/km, and 35 °C/km, respectively. The result shows that the exhumation rate increases rapidly trenchward from about 0.1 mm/yr in the Kodiak Batholith area to about 0.5-0.7 mm/yr near Ugak Island (Fig. 7). The highest exhumation rates are located in the hanging wall of the Ugak Fault.

412 We also evaluate Quaternary uplift rates across the Kodiak Islands from the elevations of
413 previously reported marine terraces, assuming they all formed at about 125 ka following Carver
414 et al. (2008). Although the marine terrace heights are likely affected by isostatic rebound
415 following regional late Pleistocene deglaciation (Carver et al., 2008), and the terrace uplift rates
416 overall are higher than the calculated exhumation rates based on the AHe ages by about 0.15-0.2
417 mm/yr, they share a similar spatial pattern (Fig. 7). This pattern is also similar to the pattern
418 revealed by current geodetic data, which shows the largest spatial gradient in the trenchward
419 coastal area of the Kodiak Islands (Carver et al., 2008). The similarity of deformation patterns
420 over decadal time spans represented by geodetics, millennial time scale recorded by marine
421 terraces, and Myr time scale recorded by thermochronology suggests that the present
422 deformation mechanism has controlled a persistent uplift pattern over a range of time scales.
423 Our ZHe ages and thermal modeling results, along with previous studies on rock cooling
424 history, structures, peak temperatures, and seismic reflection profiles suggest that underplating
425 along the plate interface could be the main mechanism of forearc wedge thickening in the
426 Eocene-Oligocene (Byrne, 1986; Sample and Fisher, 1986; Moore et al., 1991; Fisher and Byrne,
427 1992; Ye et al., 1997; Clendenen et al., 2003; Rajič et al., 2023). Although we cannot preclude
428 the possibility of a new underplating system below the trenchward coastal area, the short
429 wavelength (~10 Myr cooling age difference and a doubling of exhumation rate across 10-15
430 km) of the across-strike changes in the AHe age and exhumation rate suggests that underplating
431 is unlikely the determining cause of the new exhumation pattern. The Pliocene AHe ages
432 spatially coincide with the documented active faults in the Narrow Cape area and are within
433 about 20 km from the fault traces of the offshore Kodiak Shelf Fault Zone (Fig. 4), suggesting
434 that this exhumation episode is mainly affected by the hanging-wall uplift of the active Kodiak

435 Shelf Fault Zone. Therefore, the initiation of the Kodiak Shelf Fault Zone is likely also 6-7 Ma.
436 This interpretation is consistent with the lithologic study of the latest Miocene-Pliocene
437 Albatross sedimentary sequence hanging-wall side of the fault zone, which suggests an upward
438 decrease in clasts from the uplifted shelf break (decrease in chert and total absence of calcareous
439 shale in the upper part) and an increase in clasts from the Kodiak Islands as well as the
440 shallowing of the depositional environment from shallow marine to terrestrial (Clendenen et al.,
441 1992). The initiation of the Kodiak Shelf Fault Zone might have uplifted the basin in its hanging
442 wall and interrupted the transport path of clasts from the shelf break.
443 Assuming that exhumation is related to throw on the Kodiak Shelf Fault Zone, our new
444 results on spatial variations in exhumation rate can place constraints on the deep geometry of the
445 fault zone. Most of the Kodiak Islands have been experiencing slow exhumation after 15 Ma,
446 and the rapid Pliocene exhumation is limited in the trenchward coastal area approximately
447 southeast of the Contact Fault, close to the main offshore Kodiak Shelf Fault Zone traces (Fig.
448 7). This pattern suggests that the landward-dipping Kodiak Shelf Fault Zone may become gently
449 dipping beneath the Kodiak Islands (Fig. 8). Assuming the varied exhumation is caused by pure
450 dip-slip along the Kodiak Shelf Fault Zone with a fault bend separating a steep frontal ramp from
451 a deeper gentle flat, we semi-quantitatively estimate the deep geometry. If we assume that the
452 exhumation is balanced by uplift and the uplift rates are the vertical components of fault-slip
453 rates, we can calculate the correspondent fault slip rate and dip of the gentle decollement for a
454 given dip of the frontal thrust ramp. We use the calculated exhumation rates of Ugak Island (0.59
455 mm/yr for an initial geothermal gradient 30 °C/km) and the Kodiak Batholith (0.1 mm/yr) as
456 uplift rates above the two fault domains. For a frontal dip of 30, 40, 50 and 60, we estimate the
457 corresponding dip-slip rates are 1.15 mm/yr, 0.90 mm/yr, 0.75 mm/yr and 0.67 mm/yr,

458 respectively, and the corresponding dips of the fault flat beneath the Kodiak Islands are 4.73,
459 6.09, 7.26 and 8.21 respectively (Fig. 7). Assuming the bisector of the fault bend projects to the
460 exhumation rate change at the surface, we can construct the general fault geometry. These slip
461 rate estimations do not include lateral strike-slip components, but this simplification does not
462 affect geometry estimations because only dip-direction slip contributes to the uplift. We find that
463 even a steep 60-degree Kodiak Shelf Fault Zone frontal thrust cannot directly connect to the
464 subduction interface (Hayes et al., 2018) before it becomes flat and subparallel to the interface at
465 a depth of about 20 km. The more realistic 30-degree frontal thrust requires the fault flattening at
466 a depth of about 12 km. The flat sector can be approximately correlated to an abrupt change in
467 the seismically-determined Vp/Vs ratio within the wedge (Fig. 8, Wang et al., 2024). Therefore,
468 the fault is likely to root into deep structures and may be associated with mechanical property
469 changes within the wedge rather than the subduction interface. The Contact Fault, which played
470 a similar role to the KSFZ as an old out-of-sequence thrust fault, may have been offset by
471 younger faults or the active KSFZ at depths. If its shallow part is active, it may branch into the
472 KSFZ flat. A 30-degree frontal thrust of the KSFZ also requires a fault slip rate of 1.15 mm/yr,
473 which is about 2% of the present plate convergence rate of 57 mm/yr (DeMets et al., 1990). If so,
474 only a small portion of the plate convergence has been accommodated by the Kodiak Shelf Fault
475 Zone since its presumed initiation at 6-7 Ma. Elliott and Freymueller (2020) estimated GPS-data-
476 derived left-lateral and compressional deformation rates of 2.2 ± 0.3 mm/yr and 3.5 ± 0.4 mm/yr,
477 respectively, approximately across the Kodiak Shelf Fault Zone. The much higher geodetic
478 compressional rate than our estimated long-term dip-slip rate may suggest only a portion of the
479 interseismic strain translates to permanent deformation as fault slip along the Kodiak Shelf Fault,

assuming the compression remained at a higher rate throughout the history of the Kodiak Shelf Fault.

At shallow depths, the displacement may be distributed along multiple strands. Ramos et al. (2022) previously recognized the Ugak Fault, the primary offshore strand of the Kodiak Shelf Fault Zone, from bathymetry data and legacy seismic profiles. Using recent bathymetry data and archived seismic images collected in 1975, we mapped more active fault strands in the Ugak Island area (Figs. 3 and S1). They exhibit linear fault and/or fold scarps on the surface. On the seismic reflective images, they offset young deposits and occasionally show growth strata. Seismic images also show the Ugak Fault has the most prominent offset (Fig. S1). A previous onshore geomorphologic and paleoseismological studies (Carver et al., 2008) and our bedrock-structure survey along the coastal cliff in the Narrow Cape area also highlight multiple high-angle faults. The high-angle faults we observed are in the core of a broad 3-km wide anticline formed within the Narrow Cape Formation and its underlying unconformity. We interpret them as shallow faults accommodating passive deformation above a blind thrust fault strand below the broad anticline or as fault strands that mainly accommodate strike-slip displacement and may merge together at depth (Fig. 8).

5.3. Kodiak Shelf Fault Zone Development Mechanism

Reactivation of inherited structures as a mechanism for upper-plate out-of-sequence thrusting is common in many accretionary complexes, such as the Shimanto accretionary complex in Japan (Fisher et al., 2019). The development of the Kodiak Shelf Fault Zone may have exploited the preexisting upper-plate lithologic architecture. The fault system has developed along an approximate boundary in the forearc between lithologies of different mechanical properties (Fig. 8). At shallow levels, the landward side of the fault system is mainly composed

503 of stronger, less permeable and porous underplated and accreted metamorphosed and igneous
504 rocks, such as the Ghost Rocks Formation, the Kodiak Formation, igneous plutons, and the late
505 Triassic to early Jurassic accretionary complex. The trenchward side of the fault system is
506 mainly composed of weaker, more permeable and porous accreted rocks that offscraped from the
507 subduction plate represented by the Sitkalidak Formation and younger units (Moore and
508 Allwardt, 1980; Byrne and Fisher, 1987). The first-order across-fault lithology and mechanical
509 property changes are also exhibited by a low seismically-determined Vp/Vs ratio on the
510 landward side and an increased Vp/Vs ratio on the trenchward side, where the higher Vp/Vs
511 values are usually interpreted as indicative of elevated fluid content (Wang et al., 2024). The
512 strong contrast in mechanical properties is also suggested by the across-strike changes in seismic
513 velocity, gravity and magnetic field data (Song and Simons, 2003; Wells et al., 2003; Ramos et
514 al., 2022; Wang et al., 2024).
515 At depths beneath the Kodiak Islands, our estimated fault flat of the Kodiak Shelf Fault is
516 located approximately where there is an abrupt low-to-high gradient in the seismically-
517 determined Vp/Vs ratio at depths of about 15-20 km within the wedge (Fig. 8). Because the
518 duplex structure may have developed through the mainly Eocene-Oligocene underplating process
519 beneath the Kodiak Islands, the change in Vp/Vs ratio may represent the roof of the duplex
520 structure, i.e., the contact between the underplated material and the stronger, less permeable and
521 porous metamorphosed and igneous rocks exposed at the surface. The low porosity-permeability
522 rocks, indicated by low Vp/Vs values, in the upper crustal part of the wedge may have facilitated
523 the trapping of fluids released from the dehydration of the subducting slab within the underplated
524 rocks, which are characterized by high Vp/Vs values. On the EDGE deep seismic reflection
525 image, approximately 100 km northeast of the Kodiak Islands, a deep arch-shaped high-to-low

526 transition of seismic velocity similar to the deep Vp/Vs ratio change in the Kodiak Islands area
527 has been identified and interpreted as the top of the low-velocity underplated material (Fig. 8;
528 Moore et al., 1991; Ye et al., 1997). Therefore, although speculative, it is possible that the flat
529 part of the Kodiak Shelf Fault Zone developed by exploiting the shear zones of the old duplex
530 system, including the roof thrust. The process might have been facilitated by fluid-influenced
531 mechanical property contrast. The linkage between a similar forearc splay fault and a duplex
532 structure along the subduction interface was suggested based on the seismic images in Prince
533 William Sound, about 300 km northeast along strike (Haeussler et al., 2015).
534 Previous studies suggest that the coupling pattern and seismic behavior along the subduction
535 interface may have been significantly affected by fluid distribution because of its influence on
536 pore-fluid pressure and rheology (e.g., Shillington et al., 2015; Li et al., 2018; Fisher and Hirth,
537 2024; Wang et al., 2024). Given the coincidence between the inferred Kodiak Shelf Fault
538 geometry and the Vp/Vs pattern (Wang et al., 2024), we envision that the lithology-influenced
539 forearc fluid distribution may have facilitated the long-term continuous deformation along the
540 Kodiak Shelf Fault. Once the splay fault system was established, its damage zone may function
541 as a fluid conduit for releasing the fluid trapped beneath the low porosity-permeability rocks
542 mainly exposed on the Kodiak Islands. Although there is no direct evidence of the process along
543 this offshore fault system, a fluid-rich damage zone has been reported along an ancient out-of-
544 sequence thrust, Uganik Thrust, on the Kodiak Islands (Rowe et al., 2009). The fluid saturation
545 along the fault system can significantly reduce the yield strength and facilitate persistent long-
546 term fault activity. Because the shallow portion of the KSFZ lies above the approximate locked-
547 creeping boundary of the megathrust, earthquakes along the KSFZ may be triggered by upper-
548 plate stress changes during megathrust events. If our predicted fault geometry is correct, the

549 KSFZ could also rupture independently in upper-plate earthquakes without major megathrust
550 earthquakes.

551 6. **Conclusions**

552 Most of our ZHe ages record cooling through ZHe closure temperature in the late
553 Eocene-early Oligocene, temporally and spatially consistent with the Eocene-early Oligocene
554 broad antiformal exhumation previously documented by zircon and apatite fission track
555 thermochronological ages. However, our AHe ages reveal a new pattern; the ages record cooling
556 through AHe closure temperature from early Miocene to Pliocene and exhibit an overall decrease
557 trenchward, with Pliocene ages (3-5 Ma) collected from the trenchward coastal area of the
558 Kodiak Islands. Our thermal history modeling suggests that the trenchward coastal area of the
559 Kodiak Islands experienced a change from early-middle Miocene basin subsidence to recent
560 deformation and rapid uplift since 6-7 Ma. In contrast, the rest of the island experienced an early-
561 middle Miocene transition from the prolonged relatively rapid Eocene-Oligocene exhumation to
562 a slow exhumation phase starting approximately in the late Miocene. The early-middle Miocene
563 change in the exhumation pattern might be caused by a change in the dominant deformation
564 mechanism affecting the Kodiak Islands, from broad underplating along the subduction interface
565 to the hanging-wall uplift of the Kodiak Shelf Fault Zone, an active crustal splay fault system
566 above the down-dip edge of the seismogenic zone. The observation that the newly revealed post-
567 Miocene long-term exhumation pattern resembles the estimated uplift patterns based on elevated
568 Pleistocene marine terraces and decadal geodetic data suggests that the splay-fault-related
569 exhumation has persisted from Miocene to Recent. The inherited upper-plate structures and
570 lithologic architecture may affect the fluid distribution (and possibly pore fluid pressure), and

therefore effective rock strength in the forearc wedge in a way that facilitates the development of the Kodiak Shelf Fault and its persistent deformation over geological time.

Acknowledgements. This work was primarily funded by NSF grant EAR-2046278 to K. Morell. The authors are grateful to P. Hauessler for his insight in this work. The authors thank Fan Wang for providing the high-resolution profile of Vp/Vs data (Wang et al., 2024) used in Figure 8. The authors also thank J. Metcalf (CU TRaIL) and A. Kylander-Clark (UC Santa Barbara) for their help with the zircon and apatite (U-Th)/He dating and zircon U-Pb dating analyses, respectively. The authors thank Donna Shillington and Eva Enkelmann for their comments and suggestions that improved the manuscript.

References

Barker, D.H.N., Henrys, S., Caratori Tontini, F., Barnes, P.M., Bassett, D., Todd, E., Wallace, L., 2018. Geophysical Constraints on the Relationship Between Seamount Subduction, Slow Slip, and Tremor at the North Hikurangi Subduction Zone, New Zealand. Geophysical Research Letters 45. https://doi.org/10.1029/2018gl080259.

Barnes, P.M., Wallace, L.M., Saffer, D.M., Bell, R.E., Underwood, M.B., Fagereng, A., Meneghini, F., Savage, H.M., Rabinowitz, H.S., Morgan, J.K., Kitajima, H., Kutterolf, S., Hashimoto, Y., Engelmann de Oliveira, C.H., Noda, A., Crundwell, M.P., Shepherd, C.L., Woodhouse, A.D., Harris, R.N., Wang, M., Henrys, S., Barker, D.H.N., Petronotis, K.E., Bourlange, S.M., Clennell, M.B., Cook, A.E., Dugan, B.E., Elger, J., Fulton, P.M., Gamboa, D., Greve, A., Han, S., Hüpers, A., Ikari, M.J., Ito, Y., Kim, G.Y., Koge, H., Lee, H., Li, X., Luo, M., Malie, P.R., Moore, G.F., Mountjoy, J.J., McNamara, D.D.,

Paganoni, M., Screaton, E.J., Shankar, U., Shreedharan, S., Solomon, E.A., Wang, X., Wu, H.-Y., Pecher, I.A., LeVay, L.J., 2020. Slow slip source characterized by lithological and geometric heterogeneity. Science Advances 6, eaay3314. https://doi.org/10.1126/sciadv.aay3314.

Burns, L.E., 1985. The Border Ranges ultramafic and mafic complex, south-central Alaska: cumulate fractionates of island-arc volcanics. Canadian Journal of Earth Sciences 22, 1020-1038. https://doi.org/10.1139/e85-106.

Byrne, T., 1984. Early deformation in melange terranes of the Ghost Rocks Formation, Kodiak Islands, Alaska, in: Raymond, L.A. (Ed.), Melanges: Their Nature, Origin, and Significance. Geological Society of America, pp. 21-51.

Byrne, T., 1986. Eocene underplating along the Kodiak Shelf, Alaska: Implications and regional correlations. Tectonics 5, 403-421. https://doi.org/https://doi.org/10.1029/TC005i003p00403.

Byrne, T., Fisher, D., 1987. Episodic growth of the Kodiak convergent margin. Nature 325, 338-341. https://doi.org/10.1038/325338a0.

Carden, J.R., Connelly, W., Forbes, R.B., Turner, D.L., 1977. Blueschists of the Kodiak Islands, Alaska: An extension of the Seldovia schist terrane. Geology 5, 529-533. https://doi.org/10.1130/0091-7613(1977)5<529:Botkia>2.0.Co;2.

Carver, G., Sauber, J., Lettis, W., Witter, R., Whitney, B., Freymueller, J., 2008. Active faults on northeastern Kodiak Island, Alaska. Active tectonics and seismic potential of Alaska: American Geophysical Union Geophysical Monograph 179, 167-184

Clendenen, W.S., Fisher, D., Byrne, T., Sisson, V.B., Roeske, S.M., Pavlis, T.L., 2003. Cooling and exhumation history of the Kodiak accretionary prism, southwest Alaska, in: Sisson,

617 V.B., Roeske, S.M., Pavlis, T.L. (Eds.), Geology of a transpressional orogen developed
618 during ridge-trench interaction along the North Pacific margin. Geological Society of
619 America Special Paper 371, Boulder, Colorado, pp. 71-88.
620 Clendenen, W.S., Sliter, W.V., Byrne, T., 1992. Tectonic implications of the Albatross
621 sedimentary sequence, Sitkinak Island, Alaska, in: Bradley, D.C., Ford, A.B. (Eds.),
622 Geologic studies in Alaska by the U.S. Geological Survey, 1990, Denver, CO, pp. 52-70.
623 Connelly, W., 1978. Uyak Complex, Kodiak Islands, Alaska: A Cretaceous subduction complex.
624 GSA Bulletin 89, 755-769. https://doi.org/10.1130/0016-
625 7606(1978)89<755:UCKIAA>2.0.CO;2.
626 Cook, B.J., Henstock, T.J., McNeill, L.C., Bull, J.M., 2014. Controls on spatial and temporal
627 evolution of prism faulting and relationships to plate boundary slip offshore north-central
628 Sumatra. Journal of Geophysical Research: Solid Earth 119, 5594-5612.
629 https://doi.org/10.1002/2013jb010834.
630 Cummins, P.R., Kaneda, Y., 2000. Possible splay fault slip during the 1946 Nankai earthquake.
631 Geophysical Research Letters 27, 2725-2728.
632 https://doi.org/https://doi.org/10.1029/1999GL011139.
633 DeMets, C., Gordon, R.G., Argus, D.F., Stein, S., 1990. Current plate motions. Geophysical
634 Journal International 101, 425-478. https://doi.org/10.1111/j.1365-246X.1990.tb06579.x.
635 DePaolis, J.M., Dura, T., Witter, R.C., Haeussler, P.J., Bender, A., Curran, J.H., Corbett, D.R.,
636 2024. Repeated Coseismic Uplift of Coastal Lagoons Above the Patton Bay Splay Fault
637 System, Montague Island, Alaska, USA. Journal of Geophysical Research: Solid Earth
638 129. https://doi.org/10.1029/2023jb028552.

639 Dielforder, A., Hetzel, R., Oncken, O., 2020. Megathrust shear force controls mountain height at
640 convergent plate margins. Nature 582, 225-229. https://doi.org/10.1038/s41586-020-
641 2340-7.
642 Elliott, J., Freymueller, J.T., 2020. A Block Model of Present-Day Kinematics of Alaska and
643 Western Canada. Journal of Geophysical Research: Solid Earth 125, e2019JB018378.
644 https://doi.org/10.1029/2019JB018378.
645 Farris, D.W., 2010. Tectonic and petrologic evolution of the Kodiak batholith and the trenchward
646 belt, Kodiak Island, AK: Contact fault juxtaposition? Journal of Geophysical Research
647 115. https://doi.org/10.1029/2009jb006434.
648 Farris, D.W., Haeussler, P., Friedman, R., Paterson, S.R., Saltus, R.W., Ayuso, R., 2006.
649 Emplacement of the Kodiak batholith and slab-window migration. Geological Society of
650 America Bulletin 118, 1360-1376. https://doi.org/10.1130/b25718.1.
651 Fisher, D., Byrne, T., 1987. Structural evolution of underthrusted sediments, Kodiak Islands,
652 Alaska. Tectonics 6, 775-793. https://doi.org/10.1029/TC006i006p00775.
653 Fisher, D.M., Byrne, T., 1992. Strain variations in an ancient accretionary complex: Implications
654 for forearc evolution. Tectonics 11, 330-347. https://doi.org/10.1029/91tc01490.
655 Fisher, D.M., Hirth, G., 2024. A pressure solution flow law for the seismogenic zone:
656 Application to Cascadia. Science Advances 10, eadi7279.
657 https://doi.org/doi:10.1126/sciadv.adi7279.
658 Fisher, D.M., Tonai, S., Hashimoto, Y., Tomioka, N., Oakley, D., 2019. K-Ar Dating of Fossil
659 Seismogenic Thrusts in the Shimanto Accretionary Complex, Southwest Japan. Tectonics
660 38, 3866-3880. https://doi.org/https://doi.org/10.1029/2019TC005571.

661 Fisher, M.A., Holmes, M.L., 1980. Large-scale structure of deep strata beneath Kodiak shelf,
662 Alaska. GSA Bulletin 91, 218-224. https://doi.org/10.1130/0016-
663 7606(1980)91<218:Lsodsb>2.0.Co;2.
664 Flowers, R.M., Ketcham, R.A., Shuster, D.L., Farley, K.A., 2009. Apatite (U–Th)/He
665 thermochronometry using a radiation damage accumulation and annealing model.
666 Geochimica et Cosmochimica Acta 73, 2347-2365.
667 https://doi.org/10.1016/j.gca.2009.01.015.
668 Haeussler, P.J., Armstrong, P.A., Liberty, L.M., Ferguson, K.M., Finn, S.P., Arkle, J.C., Pratt,
669 T.L., 2015. Focused exhumation along megathrust splay faults in Prince William Sound,
670 Alaska. Quaternary Science Reviews 113, 8-22.
671 https://doi.org/10.1016/j.quascirev.2014.10.013.
672 Haeussler, P.J., Bradley, D.C., Wells, R.E., Miller, M.L., 2003. Life and death of the
673 Resurrection plate: Evidence for its existence and subduction in the northeastern Pacific
674 in Paleocene–Eocene time. GSA Bulletin 115, 867-880. https://doi.org/10.1130/0016-
675 7606(2003)115<0867:Ladotr>2.0.Co;2.
676 Hayes, G.P., Moore, G.L., Portner, D.E., Hearne, M., Flamme, H., Furtney, M., Smoczyk, G.M.,
677 2018. Slab2, a comprehensive subduction zone geometry model. Science 362, 58-61.
678 https://doi.org/10.1126/science.aat4723.
679 Jolivet, R., Simons, M., Duputel, Z., Olive, J.-A., Bhat, H.S., Bletery, Q., 2020. Interseismic
680 Loading of Subduction Megathrust Drives Long-Term Uplift in Northern Chile.
681 Geophysical Research Letters 47, e2019GL085377.
682 https://doi.org/10.1029/2019gl085377.

683 Ketcham, R.A., 2005. Forward and Inverse Modeling of Low-Temperature Thermochronometry
684 Data. Reviews in Mineralogy and Geochemistry 58, 275-314.
685 https://doi.org/10.2138/rmg.2005.58.11.
686 Kimura, G., Kitamura, Y., Hashimoto, Y., Yamaguchi, A., Shibata, T., Ujiie, K., Okamoto, S.y.,
687 2007. Transition of accretionary wedge structures around the up-dip limit of the
688 seismogenic subduction zone. Earth and Planetary Science Letters 255, 471-484.
689 https://doi.org/https://doi.org/10.1016/j.epsl.2007.01.005.
690 Li, J., Shillington, D.J., Saffer, D.M., Bécel, A., Nedimović, M.R., Kuehn, H., Webb, S.C.,
691 Keranen, K.M., Abers, G.A., 2018. Connections between subducted sediment, pore-fluid
692 pressure, and earthquake behavior along the Alaska megathrust. Geology 46, 299-302.
693 https://doi.org/10.1130/g39557.1.
694 Liberty, L.M., Brothers, D.S., Haeussler, P.J., 2019. Tsunamigenic Splay Faults Imply a Long-
695 Term Asperity in Southern Prince William Sound, Alaska. Geophysical Research Letters
696 46, 3764-3772. https://doi.org/10.1029/2018gl081528.
697 Liberty, L.M., Finn, S.P., Haeussler, P.J., Pratt, T.L., Peterson, A., 2013. Megathrust splay faults
698 at the focus of the Prince William Sound asperity, Alaska. Journal of Geophysical
699 Research: Solid Earth 118, 5428-5441. https://doi.org/10.1002/jgrb.50372.
700 Marincovich, L., Jr, Moriya, S., 1992. Early middle Miocene mollusks and benthic foraminifers
701 from Kodiak Island, Alaska, in: Bradley, D.C., Ford, A.B. (Eds.), Geologic studies in
702 Alaska by the U.S. Geological Survey, 1990, Denver, CO, pp. 163-169.
703 Michel-Wolf, L., Ehlers, T.A., Bendick, R., 2022. Transitions in subduction zone properties
704 align with long-term topographic growth (Cascadia, USA). Earth and Planetary Science
705 Letters 580. https://doi.org/10.1016/j.epsl.2021.117363.

706 Moore, G.F., Bangs, N.L., Taira, A., Kuramoto, S., Pangborn, E., Tobin, H.J., 2007. Three-
707 Dimensional Splay Fault Geometry and Implications for Tsunami Generation. Science
708 318, 1128-1131. https://doi.org/doi:10.1126/science.1147195.
709 Moore, J.C., 1978. Orientation of underthrusting during latest Cretaceous and earliest Tertiary
710 time, Kodiak Islands, Alaska. Geology 6, 209-213. https://doi.org/10.1130/0091-
711 7613(1978)6<209:Ooudlc>2.0.Co;2.
712 Moore, J.C., Allwardt, A., 1980. Progressive deformation of a Tertiary Trench Slope, Kodiak
713 Islands, Alaska. Journal of Geophysical Research: Solid Earth 85, 4741-4756.
714 https://doi.org/10.1029/JB085iB09p04741.
715 Moore, J.C., Byrne, T., Plumley, P.W., Reid, M., Gibbons, H., Coe, R.S., 1983. Paleogene
716 evolution of the Kodiak Islands, Alaska: Consequences of ridge-trench interaction in a
717 more southerly latitude. Tectonics 2, 265-293. https://doi.org/10.1029/TC002i003p00265.
718 Moore, J.C., Diebold, J., Fisher, M.A., Sample, J., Brocher, T., Talwani, M., Ewing, J., Huene,
719 R.v., Rowe, C., Stone, D., Stevens, C., Sawyer, D., 1991. EDGE deep seismic reflection
720 transect of the eastern Aleutian arc-trench layered lower crust reveals underplating and
721 continental growth. Geology 19, 420-424. https://doi.org/10.1130/0091-
722 7613(1991)019<0420:EDSRTO>2.3.CO;2 %J Geology.
723 Nilsen, T.H., Moore, G.W., 1979. Reconnaissance study of Upper Cretaceous to Miocene
724 stratigraphic units and sedimentary facies, Kodiak and adjacent islands, Alaska, with a
725 section on sedimentary petrography, in: Winkler, G.R. (Ed.), Geological Survey
726 Professional Paper 1093.

727 Oryan, B., Olive, J.-A., Jolivet, R., Malatesta, L.C., Gailleton, B., Bruhat, L., 2024. Megathrust
728 locking encoded in subduction landscapes. Science Advances 10, eadl4286.
729 https://doi.org/doi:10.1126/sciadv.adl4286.
730 Park, J.-O., Tsuru, T., Kodaira, S., Cummins, P.R., Kaneda, Y., 2002. Splay Fault Branching
731 Along the Nankai Subduction Zone. Science 297, 1157-1160.
732 https://doi.org/doi:10.1126/science.1074111.
733 Plafker, G., 1965. Tectonic Deformation Associated with the 1964 Alaska Earthquake. Science
734 148, 1675-1687. https://doi.org/doi:10.1126/science.148.3678.1675.
735 Qin, Y., Chen, J., Singh, S.C., Hananto, N., Carton, H., Tapponnier, P., 2024. Assessing the Risk
736 of Potential Tsunamigenic Earthquakes in the Mentawai Region by Seismic Imaging,
737 Central Sumatra. Geochemistry, Geophysics, Geosystems 25.
738 https://doi.org/10.1029/2023gc011149.
739 Rajič, K., Raimbourg, H., Famin, V., Moris-Muttoni, B., Fisher, D.M., Morell, K.D., Canizarés,
740 A., 2023. Exhuming an Accretionary Prism: A Case Study of the Kodiak Accretionary
741 Complex, Alaska, USA. Tectonics 42. https://doi.org/10.1029/2023tc007754.
742 Ramos, M.D., Liberty, L.M., Haeussler, P.J., Humphreys, R., 2022. Upper-plate structure and
743 tsunamigenic faults near the Kodiak Islands, Alaska, USA. Geosphere 18, 1474-1491.
744 https://doi.org/10.1130/ges02486.1.
745 Reiners, P.W., 2005. Zircon (U-Th)/He Thermochronometry. Reviews in Mineralogy and
746 Geochemistry 58, 151-179. https://doi.org/10.2138/rmg.2005.58.6.
747 Reiners, P.W., Spell, T.L., Nicolescu, S., Zanetti, K.A., 2004. Zircon (U-Th)/He
748 thermochronometry: He diffusion and comparisons with 40Ar/39Ar dating. Geochimica
749 et Cosmochimica Acta 68, 1857-1887. https://doi.org/10.1016/j.gca.2003.10.021.

750 Roeske, S.M., Mattinson, J.M., Armstrong, R.L., 1989. Isotopic ages of glaucophane schists on
751 the Kodiak Islands, southern Alaska, and their implications for the Mesozoic tectonic
752 history of the Border Ranges fault system. Geological Society of America Bulletin 101,
753 1021-1037. https://doi.org/10.1130/0016-7606(1989)101<1021:IAOGSO>2.3.CO;2.
754 Rowe, C.D., Meneghini, F., Moore, J.C., 2009. Fluid-rich damage zone of an ancient out-of-
755 sequence thrust, Kodiak Islands, Alaska. Tectonics 28.
756 https://doi.org/10.1029/2007TC002126.
757 Saillard, M., Audin, L., Rousset, B., Avouac, J.-P., Chlieh, M., Hall, S.R., Husson, L., Farber,
758 D.L., 2017. From the seismic cycle to long-term deformation: linking seismic coupling
759 and Quaternary coastal geomorphology along the Andean megathrust. Tectonics 36, 241-
760 256. https://doi.org/doi:10.1002/2016TC004156.
761 Sample, J.C., Fisher, D.M., 1986. Duplex accretion and underplating in an ancient accretionary
762 complex, Kodiak Islands, Alaska. Geology 14, 160-163. https://doi.org/10.1130/0091-
763 7613(1986)14<160:Daauia>2.0.Co;2.
764 Sample, J.C., Moore, J.C., 1987. Structural style and kinematics of an underplated slate belt,
765 Kodiak and adjacent islands, Alaska. GSA Bulletin 99, 7-20.
766 https://doi.org/10.1130/0016-7606(1987)99<7:Ssakoa>2.0.Co;2.
767 Sample, J.C., Reid, M.R., 2003. Large-scale, latest Cretaceous uplift along the Northeast Pacific
768 Rim: Evidence from sediment volume, sandstone petrography, and Nd isotope signatures
769 of the Kodiak Formation, Kodiak Islands, Alaska, in: Sisson, V.B., Roeske, S.M., Pavlis,
770 T.L. (Eds.), Geology of a transpressional orogen developed during ridge-trench
771 interaction along the North Pacific margin. Geological Society of America, p. 0.

772 Sauber, J., Carver, G., Cohen, S., King, R., 2006. Crustal deformation and the seismic cycle
773 across the Kodiak Islands, Alaska. Journal of Geophysical Research: Solid Earth 111.
774 https://doi.org/10.1029/2005JB003626.
775 Shillington, D.J., Bécel, A., Nedimović, M.R., Kuehn, H., Webb, S.C., Abers, G.A., Keranen,
776 K.M., Li, J., Delescluse, M., Mattei-Salicrup, G.A., 2015. Link between plate fabric,
777 hydration and subduction zone seismicity in Alaska. Nature Geoscience 8, 961-964.
778 https://doi.org/10.1038/ngeo2586.
779 Sibuet, J., Rangin, C., Lepichon, X., Singh, S., Cattaneo, A., Graindorge, D., Klingelhoefer, F.,
780 Lin, J., Malod, J., Maury, T., 2007. 26th December 2004 great Sumatra–Andaman
781 earthquake: Co-seismic and post-seismic motions in northern Sumatra. Earth and
782 Planetary Science Letters 263, 88-103. https://doi.org/10.1016/j.epsl.2007.09.005.
783 Song, T.-R.A., Simons, M., 2003. Large Trench-Parallel Gravity Variations Predict Seismogenic
784 Behavior in Subduction Zones. Science 301, 630-633.
785 https://doi.org/10.1126/science.1085557.
786 Strasser, M., Moore, G.F., Kimura, G., Kitamura, Y., Kopf, A.J., Lallemant, S., Park, J.-O.,
787 Screaton, E.J., Su, X., Underwood, M.B., Zhao, X., 2009. Origin and evolution of a splay
788 fault in the Nankai accretionary wedge. Nature Geoscience 2, 648-652.
789 https://doi.org/10.1038/ngeo609.
790 Suito, H., Freymueller, J.T., 2009. A viscoelastic and afterslip postseismic deformation model
791 for the 1964 Alaska earthquake. Journal of Geophysical Research: Solid Earth 114.
792 https://doi.org/10.1029/2008jb005954.

793 Suleimani, E., Freymueller, J.T., 2020. Near-Field Modeling of the 1964 Alaska Tsunami: The
794 Role of Splay Faults and Horizontal Displacements. Journal of Geophysical Research:
795 Solid Earth 125. https://doi.org/10.1029/2020jb019620.
796 van der Beek, P., Schildgen, T.F., 2023. Short communication: age2exhume – a
797 MATLAB/Python script to calculate steady-state vertical exhumation rates from
798 thermochronometric ages and application to the Himalaya. Geochronology 5, 35-49.
799 https://doi.org/10.5194/gchron-5-35-2023.
800 van Zelst, I., Rannabauer, L., Gabriel, A.A., van Dinther, Y., 2022. Earthquake Rupture on
801 Multiple Splay Faults and Its Effect on Tsunamis. Journal of Geophysical Research:
802 Solid Earth 127. https://doi.org/10.1029/2022jb024300.
803 von Huene, R., Miller, J.J., Krabbenhoeft, A., 2021. The Alaska Convergent Margin Backstop
804 Splay Fault Zone, a Potential Large Tsunami Generator Between the Frontal Prism and
805 Continental Framework. Geochemistry, Geophysics, Geosystems 22, e2019GC008901.
806 https://doi.org/10.1029/2019GC008901.
807 Wang, F., Wei, S.S., Drooff, C., Elliott, J.L., Freymueller, J.T., Ruppert, N.A., Zhang, H., 2024.
808 Fluids control along-strike variations in the Alaska megathrust slip. Earth and Planetary
809 Science Letters 633. https://doi.org/10.1016/j.epsl.2024.118655.
810 Wang, K., Hu, Y., 2006. Accretionary prisms in subduction earthquake cycles: The theory of
811 dynamic Coulomb wedge. Journal of Geophysical Research: Solid Earth 111.
812 https://doi.org/10.1029/2005jb004094.
813 Wang, X., Morgan, J., 2022. Effects of coseismic megasplay fault activity on earthquake
814 hazards: Insights from discrete element simulations. Journal of Structural Geology 155.
815 https://doi.org/10.1016/j.jsg.2022.104533.

Wells, R.E., Blakely, R.J., Sugiyama, Y., Scholl, D.W., Dinterman, P.A., 2003. Basin-centered asperities in great subduction zone earthquakes: A link between slip, subsidence, and subduction erosion? Journal of Geophysical Research: Solid Earth 108. https://doi.org/10.1029/2002jb002072.

Wendt, J., Oglesby, D.D., Geist, E.L., 2009. Tsunamis and splay fault dynamics. Geophysical Research Letters 36, n/a-n/a. https://doi.org/10.1029/2009gl038295.

Wilson, F.H., 2013. Reconnaissance geologic map of Kodiak Island and adjacent islands, Alaska. US Geological Survey.

Ye, S., Flueh, E.R., Klaeschen, D., von Huene, R., 1997. Crustal structure along the EDGE transect beneath the Kodiak shelf off Alaska derived from OBH seismic refraction data. Geophysical Journal International 130, 283-302. https://doi.org/10.1111/j.1365-246X.1997.tb05648.x.

Figure Captions

Fig 1. Geological map of Kodiak Islands area (Wilson, 2013) with sample locations and a subset of the new thermochronology ages. Zircon and apatite (U-Th)/He (ZHe and AHe) ages are new data and their sample names are labeled. Zircon Fission Track (ZFT) and apatite Fission Track (AFT) ages are from Clendenen et al. (2003). Age numbers in the same box are from the same sample. Ages within the gray dashed rectangle are shown in Fig. 2. The locked-creeping boundary is based on Elliott and Freymueller (2020). The inset map in the lower-left corner shows the details of a sample cluster. The regional map in the lower-right shows plate boundaries, rupture areas of forearc large earthquakes (circles; Davies et al., 1981; Liu et al., 2022), Quaternary faults (red lines; from U.S. Geological Survey), the main map extent (gray dashed box) and the profile line. Map units: Tnc – Narrow Cape Formation, Tsk – Sitkinak Formation, Tsi – Sitkalidak Formation, TKghm – Ghost Rocks Formation mélange unit, TKghc – Ghost Rocks Formation coherent unit, Kkd – Kodiak Formation, Tin – Paleogene intrusive rocks, Kmk – Uyak Complex, Jsch – Raspberry schist, Trqd – Triassic Afognak pluton, Trs – Triassic sedimentary unit.

Fig. 2 (a) Geological map of the main sample area with thermochronological ages. Underlined numbers indicate the youngest grain age of the sample. M1-M5 are locations of thermal history models in Fig 6. (b) Detailed map of the Narrow Cape Fm area. Active faults were mapped by Carver et al. (2008). Other map symbols are the same as Fig. 1. (c-d) Field photos show high-angle faults that cut the Narrow Cape Formation and unconformity and stereonet plots of faults, kinematic indicators and bedding at the two localities. (e) A profile along the coastal cliff shows cliff topography, unconformity elevation (black dots are field measurements), sample locations (red stars), and high-angle faults. The topographic profile is extracted along the dotted blue line in (b) and projected to a straight line subparallel to the coast.

Fig. 3 Bathymetry map (a) and topographic profiles (b-e) show the active Kodiak Shelf Fault Zone. U – up, D – down. Black arrows in b and c indicate topographic scarps. Note that profile P4 has a different scale from profile P1-P3.

Fig. 4 Thermochronology age profile. The profile starts at the offshore Ugak Fault (Distance = 186 km on Fig. 8 profile) and is made along the thick gray dash line in Fig. 1. The zircon and apatite (U-Th)/He (ZHe and AHe) ages are from this study. The zircon and apatite fission track (ZFT and AFT) ages are from Clendenen et al. (2003). The five ZHe samples closest to the Ugak Fault in the dashed gray polygon are not thermally reset for ZHe system after deposition (refer to text for details) and for each of these samples, only the youngest grain age is plotted. AFT ages at about 40 km are from the sample cluster shown in the inset map in Fig. 1. Their ages vary with elevation (see Supplementary Information). Labels M1-M5 represent the approximate locations of the thermal history models along the profile.

Fig. 5 Probability density plots of detrital zircon U-Pb ages of the Narrow Cape Formation and Sitkalidak Formation. The plots only show the ages younger than 250 Ma, which are the main component of the data. For each sample, N and n are the number of zircons analyzed and the number of ages younger than 250 Ma, respectively. The complete dataset is reported in Table S2.

Fig. 6 Thermal history modeling results using HeFTy version 1.9.3 (Ketcham, 2005). The modeled locations are shown in Figs. 2 and 4. Constraints in each model are based on geological context, geochronology and thermochronology ages (Supplementary Information), and peak temperature estimations reported by (Rajič et al., 2023).

Fig. 7 A trench-normal profile of estimated exhumation rates of apatite (U-Th)/He (AHe) samples (crosses) and uplift rates of marine terraces (upper panel) and estimated possible combinations of overall KSFZ fault geometries and slip rates by assuming various frontal dip angles (lower panel). Three sets of exhumation rate estimations assumed an initial geothermal gradient of 25 °C/km, 30 °C/km and 35°C/km (red, black and blue symbols, respectively). Gray shadow represents max-min uncertainties calculated from uncertainties of AHe ages. Marine terrace uplift rates were estimated based on the terrace elevation measurements and age assumption by Carver et al. (2008). Fault geometries and average slip rates were estimated based on the long-term exhumation rate pattern revealed by AHe ages. The profile starts at the offshore Ugak Fault (Distance = 186 km on Fig. 8 profile).

Fig. 8 A cross-section explains recent exhumation history and a structural model. The subduction interface geometry is based on Slab 2 (Hayes et al. 2018). The thick gray line is the normal-to-section projection of a major seismic velocity change documented by Ye et al. (1997) on the EDGE transect approximately 100 km northeast of the Kodiak Islands. The upper and lower ends of the locked-creeping transition are interpreted based on the subduction interface coupling coefficient in the Kodiak region reported by Elliot and Freymueller (2020). The up-dip limit of the locked segment and thrust faults (red for young or active and black for old inactive) are hypothetical and schematic. The Vp/Vs data is along a transect across the Kodiak Islands subparallel to our profile (Wang et al. 2024).

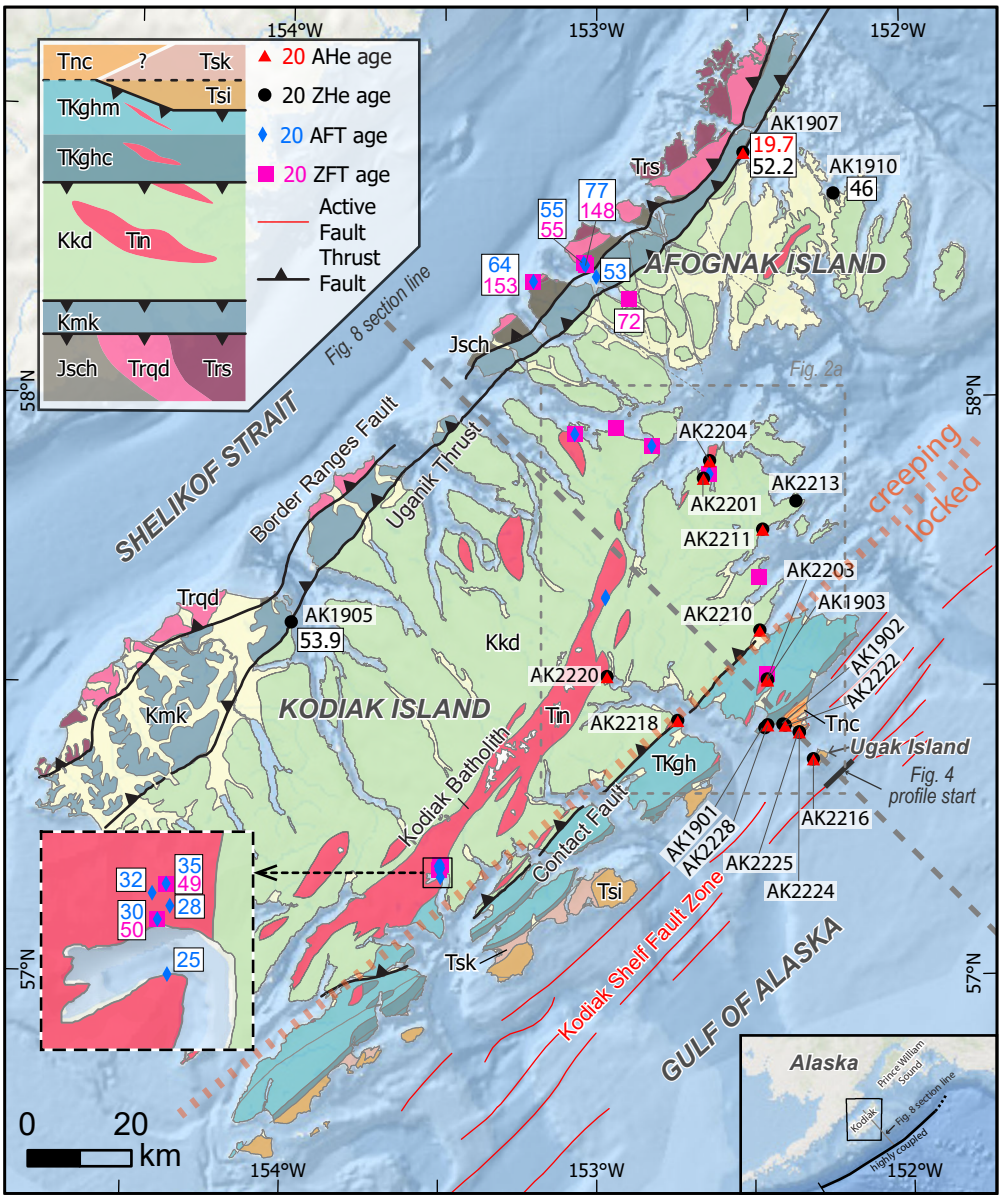
154°W
153°W
152°W
58°N
57°N
Tnc
?
Tsk
Tsi
TKghm
TKghc
Kkd
Tin
Kmk
Jsch
Trqd
Trs
20 AHe age
20 ZHe age
20 AFT age
20 ZFT age
Active Fault
Thrust Fault
Fig. 8 section line
SHELIKOF STRAIT
Border Ranges Fault
Uganik Thrust
KODIAK ISLAND
AFOGNAK ISLAND
Kodiak Batholith
Contact Fault
Kodiak Shelf Fault Zone
GULF OF ALASKA
creeping
locked
Fig. 2a
AK1907
19.7
52.2
AK1910
46
Trs
77
148
55
55
64
153
53
72
Jsch
AK2204
AK2213
AK2201
AK2211
AK2203
AK1903
AK2210
AK1902
AK2222
AK1905
53.9
Trqd
Kkd
AK2220
Kmk
Tin
AK2218
Tnc
Ugak Island
Fig. 4
profile start
TKgh
AK2216
AK1901
AK2228
AK2225
AK2224
Tsi
Tsk
32
35
49
30
50
28
25
0
20
km
Alaska
Prince William Sound
Kodiak
Fig. 8 section line
Highly coupled

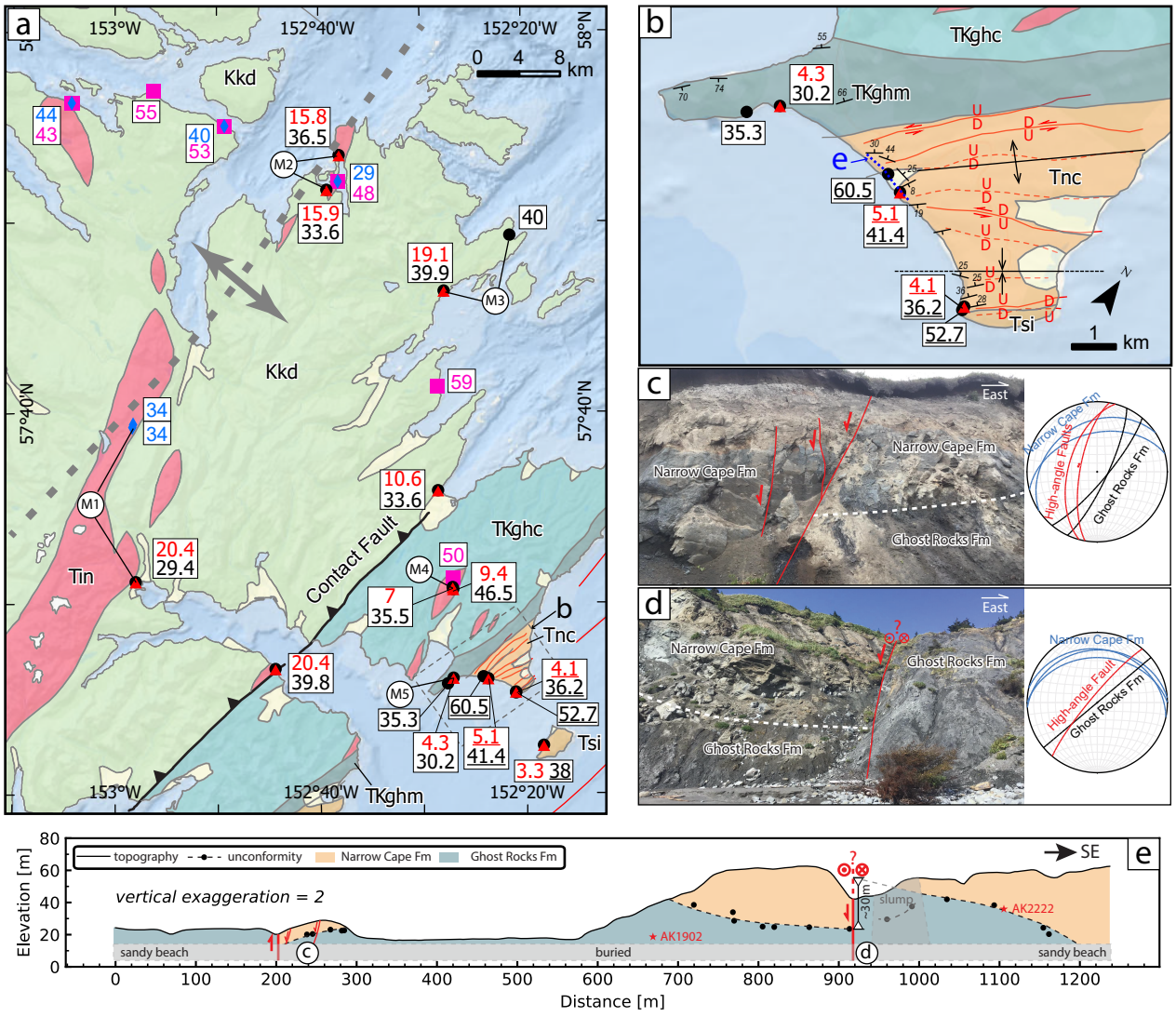
a
153°W
152°40'W
152°20'W
58°N
57°40'N
0 4 8 km
Kkd
Tin
Tnc
Tsi
TKghc
TKghm
Contact Fault
M1
M2
M3
M4
M5
44
43
55
40
53
15.8
36.5
29
48
15.9
33.6
40
19.1
39.9
59
34
34
10.6
33.6
20.4
29.4
50
9.4
46.5
7
35.5
20.4
39.8
4.1
36.2
52.7
60.5
35.3
4.3
30.2
5.1
41.4
3.3 38
b
TKghc
4.3
30.2
TKghm
35.3
e
60.5
5.1
41.4
Tnc
4.1
36.2
52.7
Tsi
1 km
c
East
Narrow Cape Fm
Ghost Rocks Fm
High-angle Faults
d
East
Narrow Cape Fm
Ghost Rocks Fm
High-angle Fault
e
topography
unconformity
Narrow Cape Fm
Ghost Rocks Fm
SE
vertical exaggeration = 2
Elevation [m]
Distance [m]
sandy beach
buried
sandy beach
AK1902
AK2222
slump
~30 m
c
d

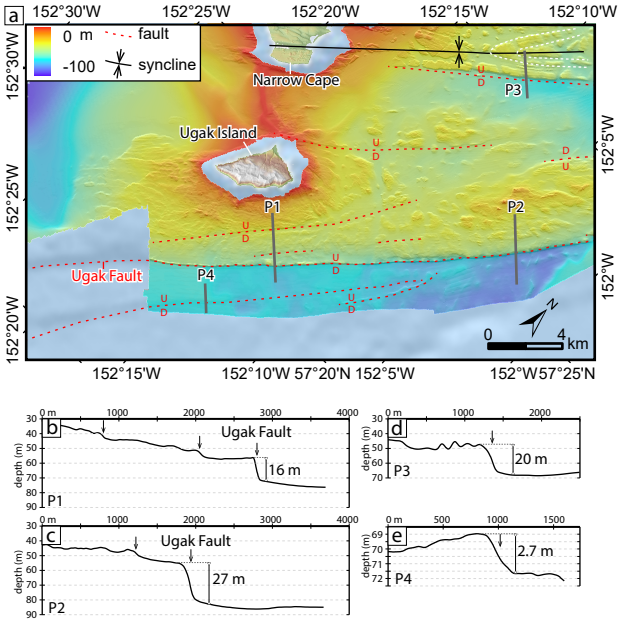
a
152°30'W
152°25'W
152°20'W
152°15'W
152°10'W
152°30'W
152°25'W
152°20'W
152°5'W
152°W
0 m
-100
fault
syncline
Narrow Cape
Ugak Island
Ugak Fault
P1
P2
P3
P4
U
D
0
4
km
152°15'W
152°10'W
57°20'N
152°5'W
152°W
57°25'N
b
Ugak Fault
16 m
P1
c
Ugak Fault
27 m
P2
d
20 m
P3
e
2.7 m
P4
depth (m)
0 m
1000
2000
3000
4000
500
1500

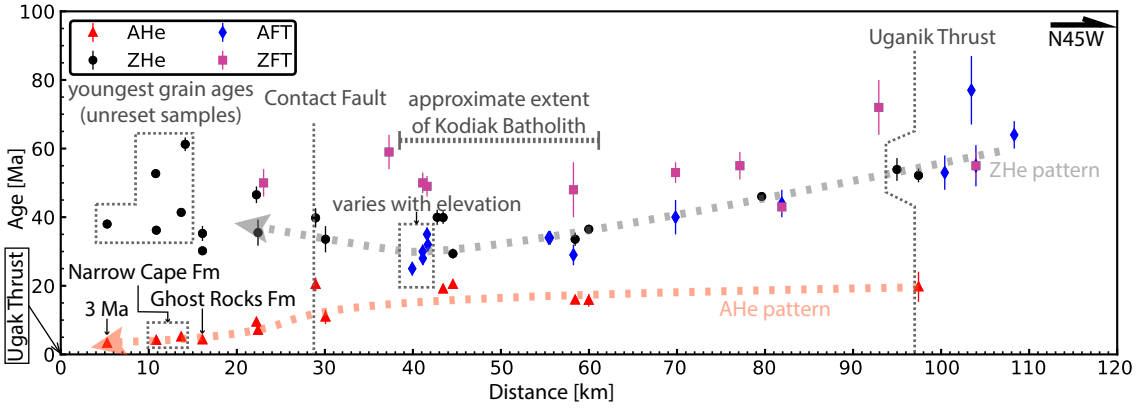
AHe
ZHe
AFT
ZFT
youngest grain ages
(unreset samples)
Contact Fault
approximate extent
of Kodiak Batholith
varies with elevation
Uganik Thrust
N45W
ZHe pattern
AHe pattern
Narrow Cape Fm
Ghost Rocks Fm
3 Ma
Ugak Thrust
Age [Ma]
Distance [km]
0
20
40
60
80
100
0
10
20
30
40
50
60
70
80
90
100
110
120

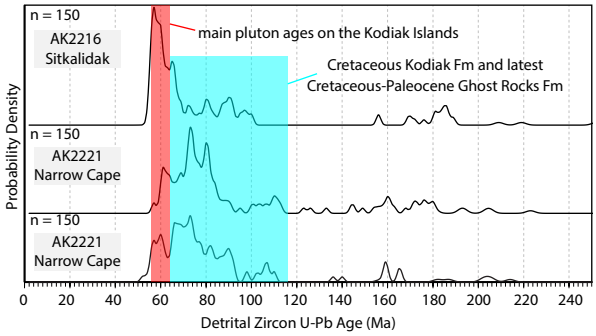
n = 150
AK2216
Sitkalidak
main pluton ages on the Kodiak Islands
Cretaceous Kodiak Fm and latest
Cretaceous-Paleocene Ghost Rocks Fm
n = 150
AK2221
Narrow Cape
n = 150
AK2221
Narrow Cape
Probability Density
0
20
40
60
80
100
120
140
160
180
200
220
240
Detrital Zircon U-Pb Age (Ma)

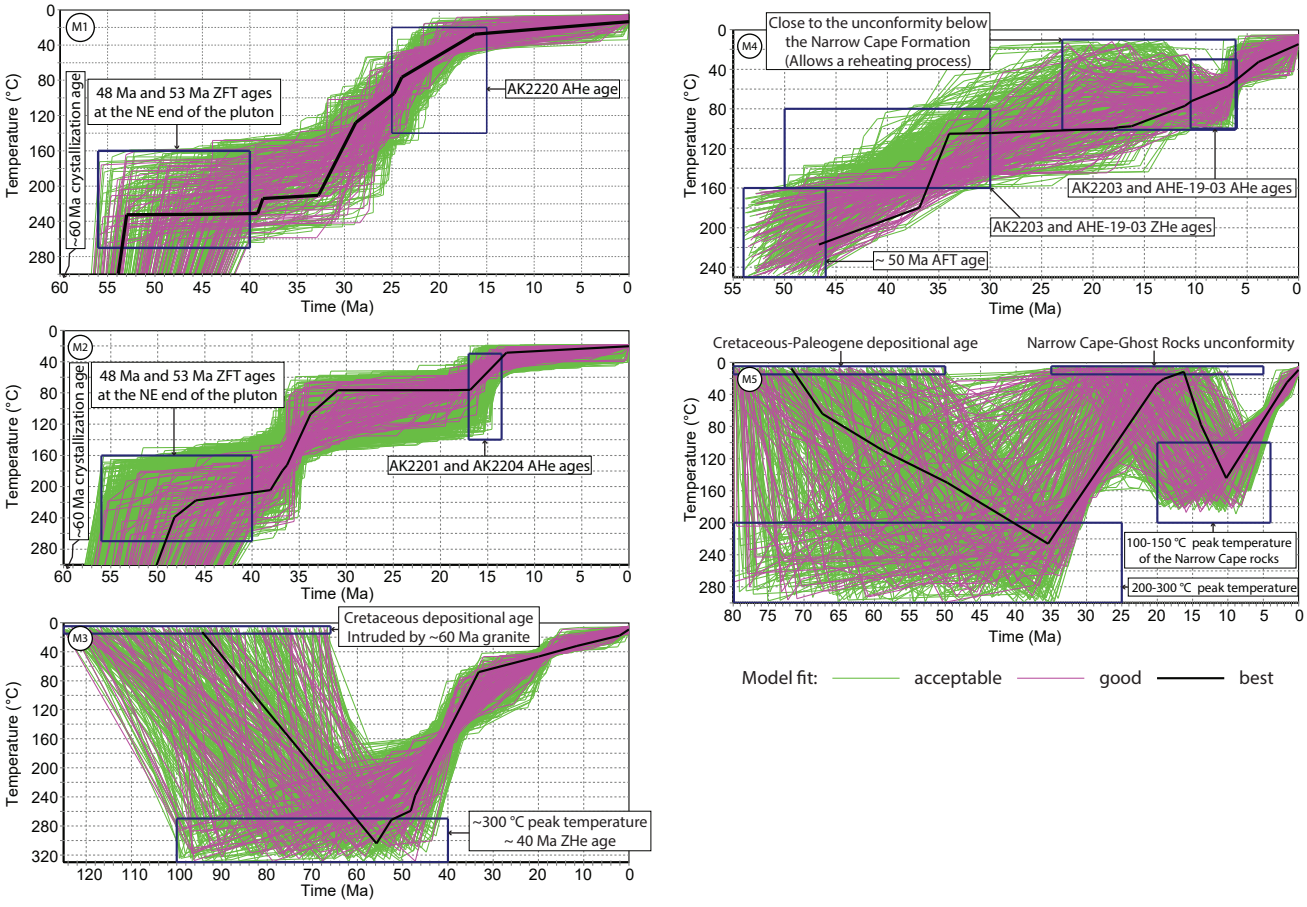
M1
48 Ma and 53 Ma ZFT ages
at the NE end of the pluton
~60 Ma crystallization age
AK2220 AHe age
Temperature (°C)
Time (Ma)
M2
48 Ma and 53 Ma ZFT ages
at the NE end of the pluton
~60 Ma crystallization age
AK2201 and AK2204 AHe ages
Temperature (°C)
Time (Ma)
M3
Cretaceous depositional age
Intruded by ~60 Ma granite
~300 °C peak temperature
~ 40 Ma ZHe age
Temperature (°C)
Time (Ma)
M4
Close to the unconformity below
the Narrow Cape Formation
(Allows a reheating process)
AK2203 and AHE-19-03 AHe ages
AK2203 and AHE-19-03 ZHe ages
~ 50 Ma AFT age
Temperature (°C)
Time (Ma)
Cretaceous-Paleogene depositional age
Narrow Cape-Ghost Rocks unconformity
M5
100-150 °C peak temperature
of the Narrow Cape rocks
200-300 °C peak temperature
Temperature (°C)
Time (Ma)
Model fit:
acceptable
good
best

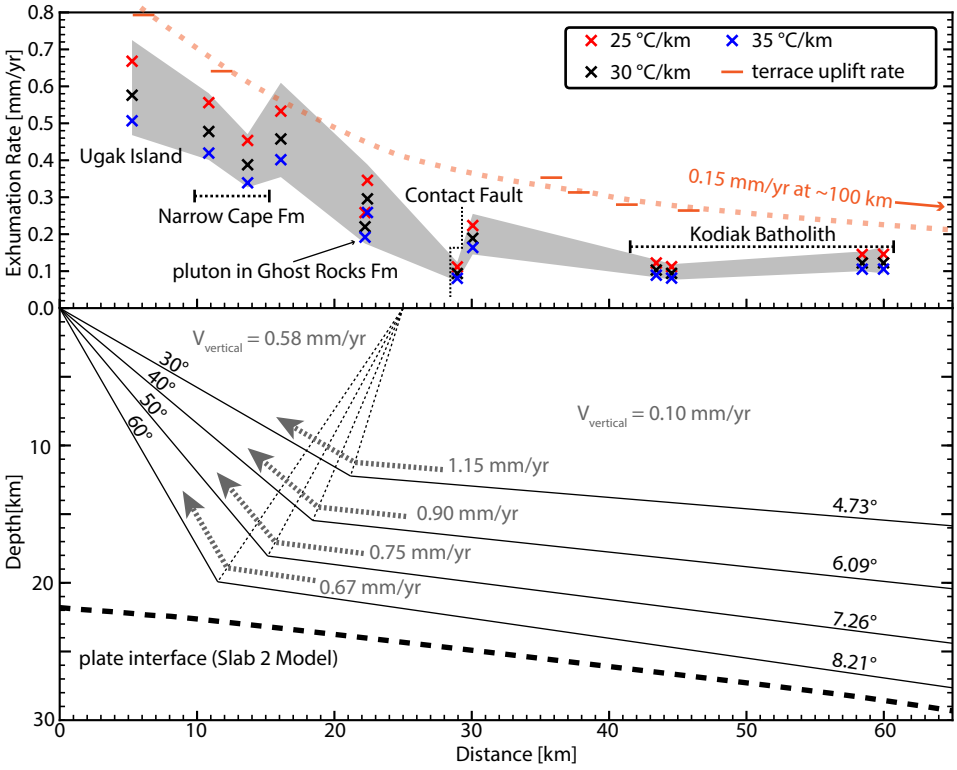
25 °C/km
35 °C/km
30 °C/km
terrace uplift rate
Exhumation Rate [mm/yr]
Ugak Island
Narrow Cape Fm
pluton in Ghost Rocks Fm
Contact Fault
0.15 mm/yr at ~100 km
Kodiak Batholith
V vertical = 0.58 mm/yr
V vertical = 0.10 mm/yr
30°
40°
50°
60°
1.15 mm/yr
0.90 mm/yr
0.75 mm/yr
0.67 mm/yr
4.73°
6.09°
7.26°
8.21°
plate interface (Slab 2 Model)
Depth[km]
Distance [km]

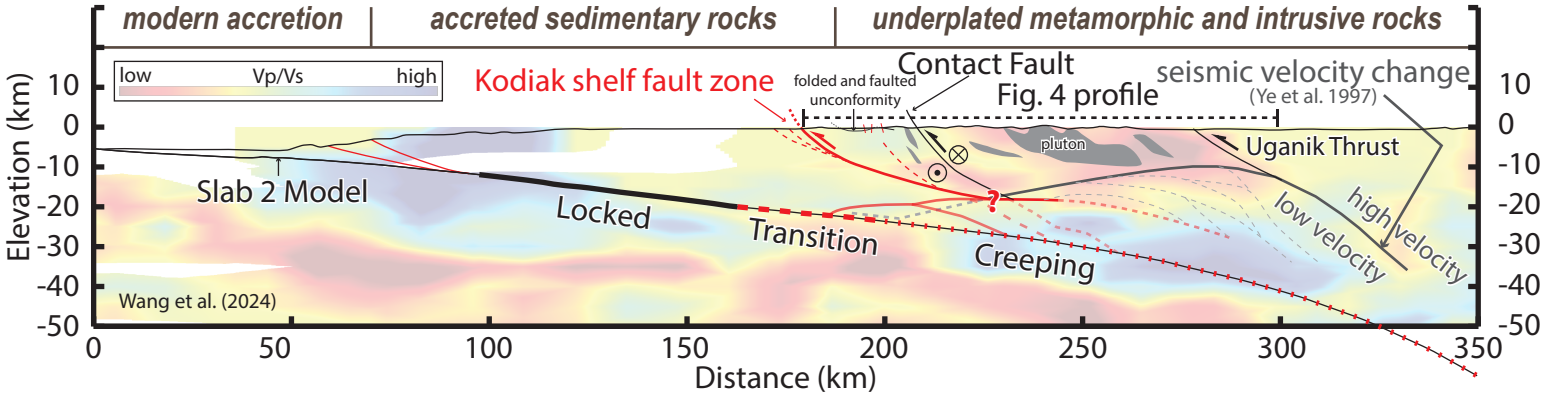
modern accretion
accreted sedimentary rocks
underplated metamorphic and intrusive rocks
low
Vp/Vs
high
Kodiak shelf fault zone
folded and faulted unconformity
Contact Fault
Fig. 4 profile
seismic velocity change
(Ye et al. 1997)
pluton
Uganik Thrust
Slab 2 Model
Locked
Transition
Creeping
low velocity
high velocity
Wang et al. (2024)
Elevation (km)
Distance (km)
10
0
-10
-20
-30
-40
-50
0
50
100
150
200
250
300
350